Eur. Phys. J. C 14, 275–284 (2000)
Digital Object Identifier (DOI) 10.1007/s100520000360

THE EUROPEAN PHYSICAL JOURNAL C

J/ψ + jet diffractive production in the direct photon process at HERA

J.-S. Xu[1], H.-A. Peng[2,3], Z.-Y. Yan[4], Z.-M. He[4]

[1] Department of Physics, Peking University, Beijing 100871, P.R. China
[2] China Center of Advance Science and Technology (World Laboratory), Beijing 100080, P.R. China
[3] Department of Physics, Peking University, Beijing 100871, P.R. China
[4] Department of Physics, Hebei Teacher's University, Shijiazhuang 050016, P.R. China

Received: 13 September 1999 / Revised version: 31 December 1999 /
Published online: 6 April 2000 – © Springer-Verlag 2000

Abstract. We present a study of the J/ψ + jet diffractive production in direct photon processes at HERA based on the factorization theorem for lepton-induced hard diffractive scattering and the factorization formalism of the non-relativistic QCD (NRQCD) for quarkonia production. Using the diffractive gluon distribution function extracted from HERA data on diffractive deep inelastic scattering and diffractive dijet photon production, we demonstrate that this process is measurable at DESY HERA. The experimental study of this process can give valuable insight in the diffractive production mechanism and test the color-octet mechanism for heavy quarkonia production in a new environment.

1 Introduction

Diffractive scattering was imported into the theory of the high energy strong interactions to explain the t distribution of elastic hadron–hadron scattering in the small $|t|$ region. In the framework of Regge theory, diffractive scattering is described in terms of the exchange of the Pomeron possessing vacuum quantum numbers [1]. However, a link between Regge theory and quantum chromodynamics (QCD) has not yet been established. To understand the diffractive production mechanism in the framework of QCD is still one of the main challenges of the strong interactions.

In an attempt to understand the underlying dynamics of diffractive interactions in terms of QCD, Low and Nussinov suggested that the Pomeron exchange corresponds to an exchange of two gluons in a color singlet [2]. But the lack of a hard scale in soft diffractive scattering makes calculations in perturbative QCD problematic. In a later development, Ingelman and Schlein [3] proposed to study diffractive scattering with a hard probe to study the partonic structure of the Pomeron experimentally. They assumed that the Pomeron, similar to the nucleon, is composed of partons, mainly of gluons, and the hard diffractive processes can probe the partonic structure of the Pomeron. Due to the nature of color-singlet exchange, diffractive scattering events are characterized by the presence of large rapidity gaps in the hadronic final state that are not exponentially suppressed. Events containing such a rapidity gap and jets were first observed by the UA8 Collaboration at CERN [4], opening the field of hard diffraction. The large rapidity gap events are also observed in the deep inelastic scattering region by the ZEUS and the H1 Collaborations at the DESY ep collider HERA [5], which offers a unique opportunity to study the diffractive processes with a hard virtual photon probe. Later on, the hard diffraction was studied in various experiments at the DESY ep collider HERA [6–8] and the Fermilab Tevatron [9]. Today, although it is still difficult to understand soft diffractive scattering in the framework of QCD, much progress in understanding the nature of hard diffraction has been made by great theoretical and experimental efforts [10]. For lepton-induced hard diffractive scattering processes such as diffractive deep inelastic scattering (DDIS) and diffractive direct photoproduction of jets, there is a factorization theorem which has been proven by Collins [11] recently. It is the same as factorization for inclusive hard processes, except that the parton densities are replaced by diffractive parton densities [12,13]. The diffractive parton densities (the primary non-perturbative quantities in hard diffraction) obey exactly the same DGLAP evolution equations as the ordinary parton densities and have been extracted from HERA data on DDIS and on diffractive photon production of jets [14]. This factorization theorem also establishes the universality of the diffractive parton distributions for those processes to which the theorem applies and hence justifies, from fundamental principles, the analysis of the ZEUS and the H1 Collaboration of hard diffraction [6–8], provided the term "Pomeron" used in these analyses is a label for a particular kind of parameterization for diffractive parton densities and is an indication of the vacuum quan-

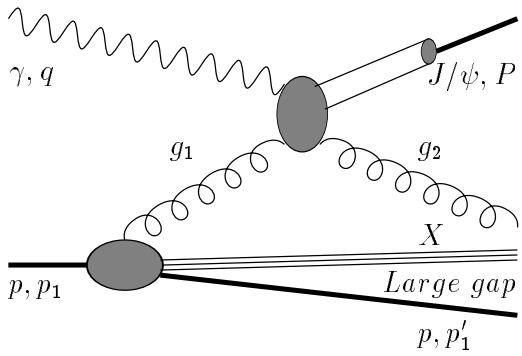

Fig. 1. Sketch diagram for J/ψ + jet diffractive production

tum numbers to be exchanged [14]. In the light of the hard diffractive factorization proven by Collins [11], the Ingelman–Schlein model for hard diffraction assumed further the factorization of diffractive parton densities into a universal Pomeron flux and Pomeron parton densities, but such a further factorization is unjustifiable from the point of view of perturbative QCD as pointed out by Ingelman in [15].

Besides this factorization approach, there are various QCD inspired models for the inclusive lepton-induced hard diffraction, such as the two-gluon exchange model [16,17], the semiclassical approach [18,19], soft color interactions [15], etc. The semiclassical approach derives leading twist diffraction from soft interactions of fast partons resulting from photon fluctuations with the proton color field in the proton rest frame. In [19] it is demonstrated that the semiclassical approach is consistent with the concept of diffractive parton distributions (i.e. the factorization approach). In the proton rest frame, the photon splits into partons ($q\bar{q}, q\bar{q}g, \cdots$) long before the interaction with the proton occurs. Before and after the interaction with the proton, this partonic system is in various configurations with small or large transverse distances. In the inclusive measurement of diffractive final states, such as the diffractive structure function of the proton (F_2^D), one sums over both these small- and large-distance configurations. In [17] a theoretical description of DDIS was formulated that interpolates between these two components. One finds that a perturbative model based on two-gluon exchange, which is valid a priori only for small-size final states and certain more exclusive diffractive processes, allows a smooth extrapolation into the soft region.

In this paper, we present a study of another hard diffractive process, diffractive J/ψ + jet production (i.e. diffractive J/ψ production at large P_{T}) in the direct photon processes at HERA:

$$\gamma(q) + p(p_1) \to p(p_1') + J/\psi(P) + \mathrm{jet} + X, \qquad (1)$$

based on the factorization theorem for lepton-induced hard diffractive scattering and the factorization formalism of the non-relativistic QCD (NRQCD) [20,21] for heavy quarkonia production. Here q, p_1, p_1', and P are the momenta of incoming photon, proton, outgoing proton, and J/ψ in the photon–proton center of mass system, respectively, X denotes the "Pomeron remnant" (Fig. 1.). The elastic J/ψ photoproduction background can be eliminated by applying suitable cuts, since J/ψ produced in an elastic process is only dominant at $P_{\mathrm{T}} < 1\,\mathrm{GeV}$ and $z > 0.9$ [22–24]. In the factorization approach, the dominant hard subprocess for diffractive J/ψ production at large P_{T} in the kinematical region we studied is photon–gluon fusion. Using the diffractive gluon distribution function extracted from HERA data on DDIS and diffractive dijet photo-production we demonstrate that this process is measurable at HERA and the experimental study of this process can give a valuable insight into the diffractive production mechanism and test the color-octet mechanism for heavy quarkonia production in a new environment. This process was briefly discussed in [25], where the relativistic corrections to photoproduction of J/ψ were studied in the color-singlet model (CSM) [26].

Our paper is organized as follows. We describe in detail our calculation scheme in Sect. 2, in which a brief introduction of the heavy quarkonium production mechanism, the hard subprocesses for J/ψ + jet production and a summary of the kinematics related to the J/ψ's z and P_{T} distributions are included. Our results and discussions are given in Sect. 3.

2 Calculation scheme

Based on the factorization theorem for lepton-induced hard diffractive scattering and the factorization formalism of NRQCD for heavy quarkonia production, the J/ψ + jet diffractive production process is shown in Fig. 1. This process consists two steps. First, the almost point-like $c\bar{c}$ pair with large P_{T} is produced in the hard subprocesses via photon–gluon fusion; then the J/ψ particle is produced from this point-like $c\bar{c}$ pair via soft interactions.

2.1 Heavy quarkonium production mechanism

Heavy quarkonium production in various processes has been the focus of much experimental and theoretical attention during the past few years [27]. This is mainly due to the observation of large discrepancies between experimental measurements of prompt and direct J/ψ production and ψ' production at large P_{T} at the Collider Detector Facility (CDF) at the Fermilab Tevatron [28] and the calculations based on CSM.

The first major conceptual advance in heavy quarkonium production was the realization that fragmentation dominates at sufficiently large P_{T} [29] which indicates that large P_{T} charmonium is mainly produced by the fragmentation of individual large P_{T} partons. The fragmentation functions are calculated in CSM. Including this fragmentation mechanism indeed yields the theoretical predictions for prompt J/ψ production at the Tevatron to within a factor of 3 of the data [30]. But the prediction for the ψ' production cross section remains a factor of 30 below

the data even after including the fragmentation contribution (the ψ' "surplus" problem). Furthermore, the presence of the logarithmic infrared divergences in the production cross sections for P wave charmonium states and the annihilation rate for $\chi_{cJ} \to q\bar{q}g$ indicates that CSM is incomplete. All this indicates that an important production mechanism beyond CSM needs to be included [31]. So the color-octet mechanism [27] is proposed which is based on the factorization formalism of NRQCD [20,21]. Contrary to the basic assumption of CSM, the heavy quark pair in a color-octet state can evolve into a physical heavy quarkonium state through soft color interactions.

Although the color-octet fragmentation picture of heavy quarkonium production [31] has provided valuable insight, the approximation that enters into fragmentation computations breaks down when the heavy quarkonium's energy becomes comparable to its mass. The fragmentation predictions for heavy quarkonium production are therefore unreliable at low $P_{\rm T}$. Based upon the above recently developed ideas in heavy quarkonium physics, Cho and Leibovich [32] identify a large class of color-octet diagrams which mediate quarkonia production and reduce to the dominant set of gluon fragmentation graphs in the high $P_{\rm T}$ limit. By fitting the data on heavy quarkonia production at the Tevatron, numerical values of the long-distance matrix elements are extracted [32,33], which are generally consistent with NRQCD power scaling rules [34]. However, in the case of inelastic J/ψ production at HERA, NRQCD with color-octet matrix elements tuned [32,33] to fit the Tevatron data predicts [35–38] at leading order a distinct rise in cross section as $z \to 1$, where z is the fraction of the photon energy transferred to the J/ψ in the proton rest frame, which is not observed by the H1 and ZEUS collaborations at HERA [23,39]. In [40], the higher-order effects due to multiple-gluon initial-state radiation and the $K_{\rm T}$ smearing effect are taken into account to solve this TEVATRON–HERA color-octet charmonium anomaly. In order to convincingly establish the color-octet mechanism, it is important to study heavy quarkonium production in other high energy processes and test the NRQCD factorization formalism. Other mechanism for heavy quarkonium production can be found in [41].

2.2 The hard subprocesses for J/ψ + jet production

J/ψ is described within the NRQCD framework in terms of Fock state decompositions by

$$\begin{aligned}|J/\psi\rangle = {} & O(1)|c\bar{c}[^3S_1^{(1)}]\rangle + O(v)|c\bar{c}[^3P_J^{(8)}]g\rangle \\ & + O(v^2)|c\bar{c}[^1S_0^{(8)}]g\rangle + O(v^2)|c\bar{c}[^3S_1^{(1,8)}]gg\rangle \\ & + O(v^2)|c\bar{c}[^3D_J^{(1,8)}]gg\rangle + \cdots, \end{aligned} \tag{2}$$

where the $c\bar{c}$ pairs are indicated within the square brackets in spectroscopic notation. The pairs' color states are indicated by singlet (1) or octet (8) superscripts. The color octet $c\bar{c}$ state can evolve into a physical J/ψ state by soft chromo-electric dipole (E1) transition(s) or chromomagnitic dipole M1 transition(s),

$$(c\bar{c})[^{2S+1}L_j^{(8)}] \to J/\psi. \tag{3}$$

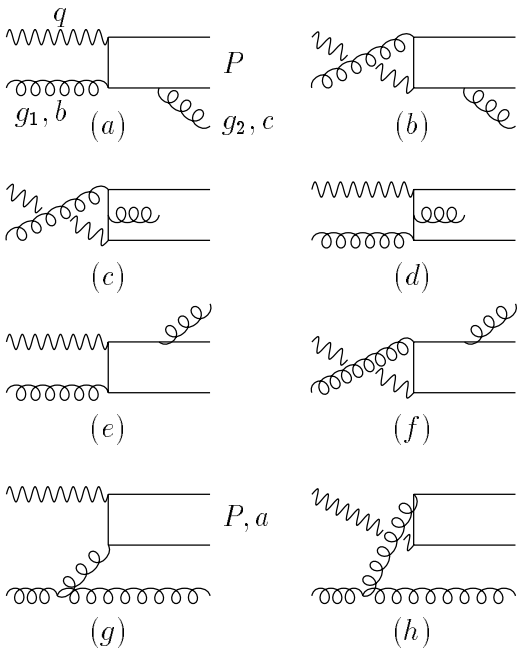

Fig. 2a–h. Feynman diagrams for $\gamma + g \to c\bar{c}[^{2S+1}L_J^{(1,8)}] + g$ subprocesses. **a**–**f** contribute to color-singlet $c\bar{c}[^3S_1^{(1)}]$ and color-octet $c\bar{c}[^3S_1^{(1)}]$ production, **a**–**h** contribute to color-octet $c\bar{c}[^1S_0^{(8)}]$ and $c\bar{c}[^3P_J^{(8)}]$ $(J = 0, 1, 2)$ production

The NRQCD factorization scheme [20] has been established to systematically separate high and low energy scale interactions. It is based upon a double power series expansion in the fine structure constant of the strong interaction, $\alpha_{\rm s}$, and the small velocity parameter v_c^2. The production of a $(c\bar{c})[^{2S+1}L_j^{(1,8)}]$ pair with separation less than or of order $1/m_c$ can be calculated perturbatively. The long-distance effects concerning the produced almost point-like $c\bar{c}$ evolving into the bound state are isolated into non-perturbative matrix elements. Furthermore, NRQCD power counting rules can be exploited to determine the dominant contributions to various quarkonium processes [34]. For direct J/ψ production, the color-octet matrix elements, $\langle 0|\mathcal{O}_8^{J/\psi}[^3S_1]|0\rangle, \langle 0|\mathcal{O}_8^{J/\psi}[^1S_0]|0\rangle$ and $\langle 0|\mathcal{O}_8^{J/\psi}[^3P_J]|0\rangle/m_c^2$ are all scaling as $m_c^3 v_c^7$. So these color-octet contributions to J/ψ production must be included for consistency.

On the partonic level, diffractive J/ψ production at large $P_{\rm T}$ is composed of photon–gluon fusion processes, which are sketched in Fig. 2. These are

$$\begin{aligned} \gamma + g &\to g + (c\bar{c})[^3S_1^{(1)}, ^3S_1^{(8)}], \quad \text{Fig. 2a–f;} \\ \gamma + g &\to g + (c\bar{c})[^1S_0^{(8)}, ^3P_J^{(8)}], \quad \text{Fig. 2a–h.} \end{aligned}$$

The quark initiated subprocesses ($\gamma q(\bar{q})$ channel) are strongly suppressed in the kinematical region we studied and will be neglected below.

The color SU(3) coefficients are given by

$$\langle 3i;\bar{3}j|1\rangle = \delta_{ji}/\sqrt{3}, \langle 3i;\bar{3}j|8a\rangle = \sqrt{2}T^a_{ji}. \quad (4)$$

Some identities involving the traces of color matrices are useful when the matrix elements are squared and spin and color averaged:

$$\begin{aligned}
\frac{1}{8}\mathrm{Tr}(T^bT^c)\mathrm{Tr}^*(T^bT^c)\frac{1}{\sqrt{3}}\frac{1}{\sqrt{3}} &= \frac{1}{12},\\
\frac{1}{8}F_c^{(a)-(c)}F_c^{*(a)-(c)} &= \frac{7}{12},\\
\frac{1}{8}F_c^{(a)-(c)}F_c^{*(d)-(f)} &= \frac{-1}{6},\\
\frac{1}{8}F_c^{(d)-(f)}F_c^{*(a)-(c)} &= \frac{-1}{6},\\
\frac{1}{8}F_c^{(d)-(f)}F_c^{*(d)-(f)} &= \frac{7}{12},\\
\frac{1}{8}F_c^{(g)-(h)}F_c^{*(h)-(h)} &= \frac{3}{2},\\
\frac{1}{8}F_c^{(g)-(h)}F_c^{*(a)-(c)} &= \frac{-3\mathrm{i}}{4},\\
\frac{1}{8}F_c^{(g)-(h)}F_c^{*(d)-(f)} &= \frac{3\mathrm{i}}{4},\\
\frac{1}{8}F_c^{*(g)-(h)}F_c^{(a)-(c)} &= \frac{3\mathrm{i}}{4},\\
\frac{1}{8}F_c^{*(g)-(h)}F_c^{(d)-(f)} &= \frac{-3\mathrm{i}}{4}. \quad (5)
\end{aligned}$$

Here

$$\begin{aligned}
F_c^{(a)-(c)} &= \sqrt{2}\mathrm{Tr}(T^aT^bT^c),\\
F_c^{(d)-(f)} &= \sqrt{2}\mathrm{Tr}(T^aT^cT^b),\\
F_c^{(g)-(h)} &= \sqrt{2}\mathrm{Tr}(T^aT^d)f_{dbc}\\
&= \frac{\sqrt{2}}{2}f_{abc}. \quad (6)
\end{aligned}$$

Note that the hard subprocesses which produce color-octet $(c\bar{c})[^1S_0^{(8)}, ^3P_J^{(8)}]$ pairs involve triple-gluon coupling (two of them are external gluons). This situation implies that we cannot use the trick of replacing the sum over gluon polarization states by

$$\sum_\lambda \varepsilon_\alpha(\lambda)\varepsilon^*_{\alpha'}(\lambda) \to -g_{\alpha\alpha'}$$

when we use the Feynman gauge for the gluon propagator [42]. One way to obtain the correct result is to insist that the polarization states of the two external gluons are physical (i.e., transverse). This is accomplished by the projection

$$\begin{aligned}
&\sum_\lambda \varepsilon_\alpha(\lambda)\varepsilon^*_{\alpha'}(\lambda)\\
&= -\left[g_{\alpha\alpha'} - \frac{n_\alpha k_{\alpha'} + n_{\alpha'}k_\alpha}{(n\cdot k)} + \frac{n^2 k_\alpha k_{\alpha'}}{(n\cdot k)^2}\right], \quad (7)
\end{aligned}$$

where n is an arbitrary 4-vector and k is the gluon 4-momentum. This is analogous to using an axial (i.e. physical) gauge for the gluon propagator. Our choice for the 4-vector n is $n = g_2$ for the incoming gluon and $n = g_1$ for the outgoing gluon; g_1, g_2 are the 4-momenta of the incoming and outgoing gluons, respectively.

With all ingredients set as above, we obtain the spin and color average-squared matrix elements $\overline{\Sigma}|M(\gamma + g \to (c\bar{c})[^{2S+1}L_j^{(1;8)}] + g)|^2$. Our analytic expressions are consistent with results of calculations carried out by Berger and Jones [26] and the results calculated from (11), (15) and appendix B of [37], but different from the expressions of [35]. For example, the expression of $\overline{\Sigma}|M(\gamma+g \to (c\bar{c})[^1S_0^{(8)}] + g)|^2$ of [35] is different from our analytic expression by a term

$$\frac{6\hat{s}\hat{u}(ee_cg_s^2)^2}{\hat{t}(\hat{s}+\hat{u})^2}, \quad (8)$$

which is exactly the contribution of the photon–ghost scattering diagram (i.e. the contribution of the unphysical polarization states of the external gluons) and should be subtracted from (A1) of [35]. Here

$$\hat{s} = (q+g_1)^2, \quad \hat{t} = (q-P)^2, \quad \hat{u} = (g_1 - P)^2. \quad (9)$$

In the Appendix, we give explicit expressions of $\overline{\Sigma}|M(\gamma + g \to (c\bar{c})[^{2S+1}L_j^{(1;8)}] + g)|^2$ for J/ψ production.

Using the spin and color average-squared matrix elements of the hard subprocesses in the NRQCD framework we obtain the sub-cross sections. The color-singlet contribution to J/ψ + jet production is well known [26]:

$$\begin{aligned}
&\frac{\mathrm{d}\hat{\sigma}}{\mathrm{d}\hat{t}}[\gamma + g \to (c\bar{c})[^3S_1^{(1)}] + g \to J/\psi + \mathrm{jet}]\\
&= \frac{1}{16\pi\hat{s}^2}\overline{\Sigma}|M(\gamma + g \to (c\bar{c})[^3S_1^{(1)}] + g)|^2\\
&\times\frac{1}{18m_c}\langle 0|\mathcal{O}_1^{J/\psi}[^3S_1]|0\rangle. \quad (10)
\end{aligned}$$

where $\langle 0|\mathcal{O}_1^{J/\psi}[^3S_1]|0\rangle$ is the color-singlet matrix element which is related to the lepton decay width of J/ψ. The average-squared matrix element $\overline{\Sigma}|M(\gamma + g \to (c\bar{c})[^3S_1^{(8)}] + g)|^2$ can be obtained from $\overline{\Sigma}|M(\gamma+g \to (c\bar{c})[^3S_1^{(1)}]+g)|^2$ by taking into account the different color factor. The color-octet $(c\bar{c})[^3S_1^{(8)}]$ contribution is

$$\begin{aligned}
&\frac{\mathrm{d}\hat{\sigma}}{\mathrm{d}\hat{t}}[\gamma + g \to (c\bar{c})[^3S_1^{(8)}] + g \to J/\psi + g]\\
&= \frac{1}{16\pi\hat{s}^2}\frac{15}{6}\overline{\Sigma}|M(\gamma + g \to (c\bar{c})[^3S_1^{(1)}] + g)|^2\\
&\times\frac{1}{24m_c}\langle 0|\mathcal{O}_8^{J/\psi}[^3S_1]|0\rangle. \quad (11)
\end{aligned}$$

The color-octet $(c\bar{c})[^3S_0^{(8)}]$ and $(c\bar{c})[^3P_J^{(8)}]$ contributions are

$$\begin{aligned}
&\frac{\mathrm{d}\hat{\sigma}}{\mathrm{d}\hat{t}}[\gamma + g \to (c\bar{c})[^1S_0^{(8)}] + g \to J/\psi + \mathrm{jet}]\\
&= \frac{1}{16\pi\hat{s}^2}\overline{\Sigma}|M(\gamma + g \to (c\bar{c})[^1S_0^{(8)}] + g)|^2
\end{aligned}$$

$$\times\frac{1}{8m_c}\langle 0|\mathcal{O}_8^{J/\psi}[^1S_0]|0\rangle,$$
$$\frac{\mathrm{d}\hat{\sigma}}{\mathrm{d}\hat{t}}[\gamma+g\to(c\bar{c})[^3P_J^{(8)}]+g\to J/\psi+\mathrm{jet}]$$
$$=\frac{1}{16\pi\hat{s}^2}\sum_J\overline{\Sigma}|M(\gamma+g\to(c\bar{c})[^3P_J^{(8)}]+g)|^2$$
$$\times\frac{1}{8m_c}\langle 0|\mathcal{O}_8^{J/\psi}[^3P_0]|0\rangle, \quad (12)$$

where the heavy quark spin symmetry

$$\langle 0|\mathcal{O}_8^{J/\psi}[^3P_J]|0\rangle=(2J+1)\langle 0|\mathcal{O}_8^{J/\psi}[^3P_0]|0\rangle \quad (13)$$

is exploited.

2.3 The z and P_T distributions of J/ψ

Now we consider the z and P_T distribution of J/ψ produced in the process (1). Based on the factorization theorem for the lepton-induced hard diffractive hard scattering [11], the differential cross section can be expressed in terms of the diffractive parton distribution [12,13] by

$$\mathrm{d}\sigma=\frac{\mathrm{d}f_{g/p}^{\mathrm{diff}}(x_1,x_{\mathbb{P}},t,\mu)}{\mathrm{d}x_{\mathbb{P}}\mathrm{d}t}\mathrm{d}x_{\mathbb{P}}\mathrm{d}t\cdot\frac{\mathrm{d}\hat{\sigma}(\gamma+g\to J/\psi+\mathrm{jet})}{\mathrm{d}\hat{t}}\mathrm{d}x_1\mathrm{d}\hat{t}. \quad (14)$$

Here

$$\frac{\mathrm{d}f_{g/p}^{\mathrm{diff}}(x_1,x_{\mathbb{P}},t,\mu)}{\mathrm{d}x_{\mathbb{P}}\mathrm{d}t}\mathrm{d}x_1 \quad (15)$$

represents the probability of finding in the proton a gluon carrying momentum faction x_1, while leaving the proton intact except for having been diffractively scattered with the momentum transfer $(x_{\mathbb{P}},t)$. $x_{\mathbb{P}}$ is the fractional momentum loss of the diffracted proton, i.e., $x_{\mathbb{P}}\simeq(p_{1z}-p'_{1z})/p_z$, and t is the invariant momentum transfer for the diffracted proton, i.e., $t=(p_1-p'_1)^2, |t|\le 1.0\,\mathrm{GeV}^2$.

We now consider the kinematics. It is convenient to introduce the variable

$$z\equiv\frac{p_1\cdot P}{p_1\cdot q}. \quad (16)$$

In terms of z and P_T (the transverse momentum of J/ψ in the photon–proton center of mass system), the Mandelstam variables and x_1 can be expressed as follows:

$$\hat{s}=\frac{P_\mathrm{T}^2}{z(1-z)}+\frac{m_\psi^2}{z},$$
$$\hat{t}=-\frac{(1-z)m_\psi^2+P_\mathrm{T}^2}{z},$$
$$\hat{u}=-\frac{P_\mathrm{T}^2}{1-z},$$
$$x_1=\frac{\hat{s}}{s_{\gamma p}}. \quad (17)$$

Here, $s_{\gamma p}=(q+p)^2$. The double differential cross section is

$$\frac{\mathrm{d}\sigma}{\mathrm{d}z\mathrm{d}P_\mathrm{T}}=\int_{x_1}^{x_{\mathbb{P}\mathrm{max}}}\mathrm{d}x_{\mathbb{P}}\int_{-1}^{0}\mathrm{d}t\frac{\mathrm{d}f_{g/p}^{\mathrm{diff}}(x_1,x_{\mathbb{P}},t,\mu)}{\mathrm{d}x_{\mathbb{P}}\mathrm{d}t}\cdot\frac{\mathrm{d}\hat{\sigma}(\gamma+g\to J/\psi+\mathrm{jet})}{\mathrm{d}\hat{t}}J\left(\frac{x_1\hat{t}}{zP_\mathrm{T}}\right), \quad (18)$$

where the Jacobian can be obtained from (17),

$$J\left(\frac{x_1\hat{t}}{zP_\mathrm{T}}\right)=\frac{2P_\mathrm{T}\hat{s}}{z(1-z)s_{\gamma p}}. \quad (19)$$

The allowed regions of z, P_T are given by

$$0\le P_\mathrm{T}\le\sqrt{(1-z)(zx_{\mathbb{P}\mathrm{max}}s_{\gamma p}-m_\psi^2)},$$
$$z_{\min}\le z\le z_{\max}, \quad (20)$$

with

$$z_{\max}=\frac{1}{2x_{\mathbb{P}\mathrm{max}}s_{\gamma p}}[x_{\mathbb{P}\mathrm{max}}s_{\gamma p}+m_\psi^2+\sqrt{(x_{\mathbb{P}\mathrm{max}}s_{\gamma p}-m_\psi^2)^2-4x_{\mathbb{P}\mathrm{max}}s_{\gamma p}P_\mathrm{T}^2}],$$
$$z_{\min}=\frac{1}{2x_{\mathbb{P}\mathrm{max}}s_{\gamma p}}[x_{\mathbb{P}\mathrm{max}}s_{\gamma p}+m_\psi^2-\sqrt{(x_{\mathbb{P}\mathrm{max}}s_{\gamma p}-m_\psi^2)^2-4x_{\mathbb{P}\mathrm{max}}s_{\gamma p}P_\mathrm{T}^2}]. \quad (21)$$

In order to suppress the Reggeon contributions, we set $x_{\mathbb{P}\mathrm{max}}=0.05$ as usual.

3 Numerical results and discussions

For numerical predictions, we use $m_c=1.5\,\mathrm{GeV}$, $\Lambda_4=235\,\mathrm{MeV}$, and set the factorization scale and the renormalization scale both equal to the transverse mass of J/ψ, i.e., $\mu^2=m_\mathrm{T}^2=(m_\psi^2+P_\mathrm{T}^2)$. The value of the color-singlet matrix element $\langle 0|\mathcal{O}_1^{J/\psi}[^3S_1]|0\rangle=1.16\,\mathrm{GeV}^3$ has been calculated from the J/ψ wave function at the origin as obtained in the QCD-motivated potential model of [43] and tabulated in [44]. The color-octet matrix elements $\langle 0|\mathcal{O}_8^{J/\psi}[^3S_1]|0\rangle$, and a linear combination of $\langle 0|\mathcal{O}_8^{J/\psi}[^1S_0]|0\rangle$ and $\langle 0|\mathcal{O}_8^{J/\psi}[^3P_0]|0\rangle$, $M_k=\langle 0|\mathcal{O}_8^{J/\psi}[^1S_0]|0\rangle+(k/m_c^2)\langle 0|\mathcal{O}_8^{J/\psi}[^3P_0]|0\rangle$, have been extracted from CDF measurements by several groups [32,33,40,45]. The theoretical uncertainties in the extraction of these matrix elements are due to ambiguities in the choice of the renormalization and factorization scale, the charm quark mass and the parton distribution set, and uncertainties of the magnitude of higher-order α_s and v_c^2 corrections, etc. The value of M_k is very sensitive to various effects which can modify the shape of the P_T spectrum of J/ψ. At present the diffractive parton distributions and the matrix elements we used are all of leading order in α_s; hence, for consistency, we use the leading-order color-octet matrix

elements determined by Beneke and Krämer [33] from fitting the direct J/ψ production data at the Tevatron using the GRV LO parton distribution functions [46],

$$\langle 0|\mathcal{O}_8^{J/\psi}[^3S_1]|0\rangle = 1.12\times 10^{-2}\,\mathrm{GeV}^3,$$
$$\langle 0|\mathcal{O}_8^{J/\psi}[^1S_0]|0\rangle + \frac{3.5}{m_c^2}\langle 0|\mathcal{O}_8^{J/\psi}[^3P_0]|0\rangle = 3.90\times 10^{-2}\,\mathrm{GeV}^3. \quad (22)$$

Since the matrix elements $\langle 0|\mathcal{O}_8^{J/\psi}[^1S_0]|0\rangle$ and $\langle 0|\mathcal{O}_8^{J/\psi}[^3P_0]|0\rangle$ are not determined separately, we choose $\langle 0|\mathcal{O}_8^{J/\psi}[^1S_0]|0\rangle = 1.0\times 10^{-2}\,\mathrm{GeV}^3$ as in [23,38] and determine the value of $\langle 0|\mathcal{O}_8^{J/\psi}[^3P_0]|0\rangle$ from (22), i.e. $\langle 0|\mathcal{O}_8^{J/\psi}[^3P_0]|0\rangle/m_c^2 = 8.3\times 10^{-3}\,\mathrm{GeV}^3$. In NRQCD, $\langle 0|\mathcal{O}_1^{J/\psi}[^3S_1]|0\rangle$ scales as $m_c^3 v_c^3$; $\langle 0|\mathcal{O}_8^{J/\psi}[^3S_1]|0\rangle$, $\langle 0|\mathcal{O}_8^{J/\psi}[^1S_0]|0\rangle$ and $\langle 0|\mathcal{O}_8^{J/\psi}[^3P_J]|0\rangle/m_c^2$ are all scaling as $m_c^3 v_c^7$, i.e. these color-octet matrix elements are suppressed by v_c^4 compared to the color-singlet matrix element – for charmonium, $\langle v_c^2\rangle \simeq 0.23$ [43,44] – so the values of the color-octet matrix elements we used are consistent with the NRQCD power counting rule. The diffractive gluon distribution function

$$\frac{\mathrm{d}f_{g/p}^{\mathrm{diff}}(x_1, x_{\mathbb{P}}, t, \mu)}{\mathrm{d}x_{\mathbb{P}}\mathrm{d}t}$$

at $\mu^2 = 4\,\mathrm{GeV}^2$ has been extracted from data on DDIS and on diffractive photoproduction of jets at HERA in [14],

$$\frac{\mathrm{d}f_{g/p}^{\mathrm{diff}}(x_1, x_{\mathbb{P}}, t, \mu^2 = 4\,\mathrm{GeV}^2)}{\mathrm{d}x_{\mathbb{P}}\mathrm{d}t} = \frac{9\beta_0^2}{4\pi^2}\left[\frac{4m_p^2 - 2.8t}{4m_p^2 - t}\left(\frac{1}{1-t/0.7}\right)^2\right] x_{\mathbb{P}}^{-2\alpha(t)}\cdot a_g(1-x_1/x_{\mathbb{P}}), \quad (23)$$

and evolves in μ^2 according to the DGLAP evolution equations [11]. Here $\beta_0 = 1.8\,\mathrm{GeV}^{-1}$, $\alpha(t) = 1.14 + 0.25t$, $a_g = 4.5\pm 0.5$. We use the central value of a_g for numerical calculation. Since, the cross section of the J/ψ elastic photoproduction (with or without proton dissociation) falls exponentially with t ($\simeq P_{\mathrm{T}}$ in elastic photoproduction) and the produced J/ψ is dominant at $P_{\mathrm{T}} < 1\,\mathrm{GeV}$ and $z > 0.9$ [22–24], in the following a P_{T} cut $P_{\mathrm{T}} \geq 1.0\,\mathrm{GeV}$ is imposed to strongly suppress this contribution. If statistics is not a limitation, it might be preferable to use a higher P_{T} cut to further suppress the higher-twist contributions.

In Fig. 3 we show the z distribution $d\sigma/dz$ of J/ψ produced in process (1) at HERA at a typical energy $s_{\gamma p}^{1/2} = 100\,\mathrm{GeV}$ and with a P_{T} cut $P_{\mathrm{T}} \geq 1.0\,\mathrm{GeV}$. The thin dash-dotted and short dashed lines represent the color-singlet contribution and the sum of the color-singlet and color-octet contributions, respectively. We observe that for $z > 0.3$ the color-singlet contribution is about the order of 10^0 nb. For completeness, in Fig. 3 we also show the z distribution of J/ψ inelastic production $\gamma + p \to J/\psi + \mathrm{jet} + X$ in the same kinematic region (upper part). In this case, the thick solid and dotted curves are the sum of the color-singlet and color-octet contributions, and the color-singlet contribution, respectively. In both cases, including the color-octet contributions, the z distributions are strongly enhanced in the high z region due to the gluon propagator in the color-octet channel (Fig. 2g,h). In the inelastic case, this behavior of rapid growing at high z does not agree with the HERA data [23,39]. However, this discrepancy should not be interpreted as a failure of the NRQCD theory itself, but rather as a failure of the leading-order approximation in α_{s} and v_c^2 for the color-octet contributions in the z region close to the boundary of phase space [37,47].

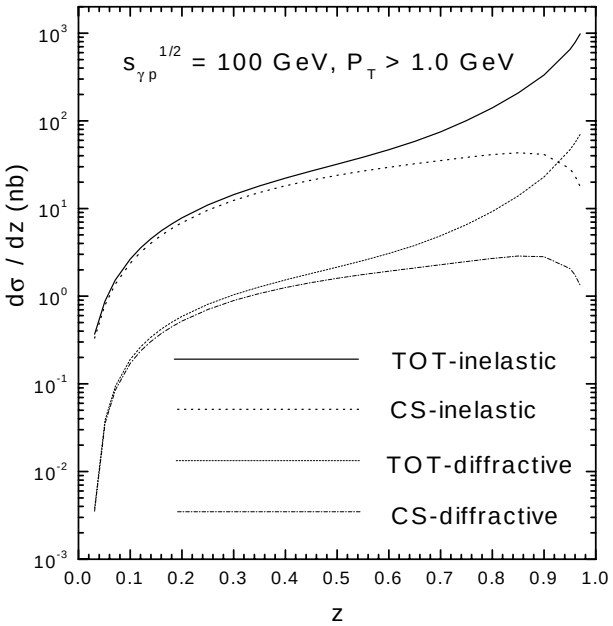

Fig. 3. z distribution $\mathrm{d}\sigma/\mathrm{d}z$ for J/ψ + jet photoproduction at HERA at $s_{\gamma p}^{1/2} = 100\,\mathrm{GeV}$, integrated over the J/ψ transverse momentum P_{T} with a lower P_{T} cut $P_{\mathrm{T}} \geq 1.0\,\mathrm{GeV}$. The thin dash-dotted and short dashed lines represent the color-singlet contribution and the sum of the color-singlet and color-octet contributions to J/ψ + jet diffractive photoproduction $\gamma + p \to J/\psi + \mathrm{jet} + p + X$ respectively. The thick solid and dotted lines curves are the sum of the color-singlet and color-octet contributions and the color-singlet contribution to inelastic J/ψ + jet photoproduction $\gamma + p \to J/\psi + \mathrm{jet} + X$, respectively

In Fig. 4, we show the P_{T} distribution $\mathrm{d}\sigma/\mathrm{d}P_{\mathrm{T}}$ at HERA with $s_{\gamma p}^{1/2} = 100\,\mathrm{GeV}$ and a z cut $0.2 \leq z \leq 0.8$. Here, the lower cut in z is employed in order to reduce the background from the resolved photon processes. The codes for the curves are the same as Fig. 3. We find that for the J/ψ + jet diffractive photoproduction in process (1) the color-octet contributions are larger than the color-singlet contribution for $P_{\mathrm{T}} > 2.6\,\mathrm{GeV}$.

In Fig. 5, we show the J/ψ + jet diffractive photoproduction cross section as a function of $s_{\gamma p}^{1/2}$ with the cuts, $P_{\mathrm{T}} \geq 1.0\,\mathrm{GeV}$, $0.2 \leq z \leq 0.8$. We observe that in the

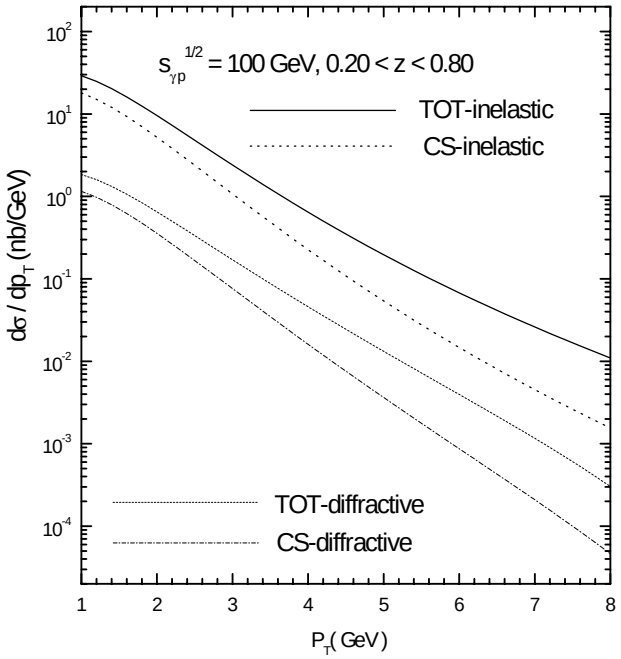

Fig. 4. Transverse momentum ($P_{\rm T}$) distribution $\mathrm{d}\sigma/\mathrm{d}P_{\rm T}$ for J/ψ + jet photoproduction at HERA at $s_{\gamma p}^{1/2} = 100\,\mathrm{GeV}$, integrated over z with a z cut $0.2 \le z \le 0.8$. The thin dash-dotted and short dashed lines represent the color-singlet contribution and the sum of the color-singlet and color-octet contributions to J/ψ + jet diffractive photoproduction $\gamma + p \to J/\psi + \mathrm{jet} + p + X$, respectively. The thick solid and dotted lines curves are the sum of the color-singlet and color-octet contributions and the color-singlet contribution to inelastic J/ψ+jet photoproduction $\gamma + p \to J/\psi + \mathrm{jet} + X$, respectively

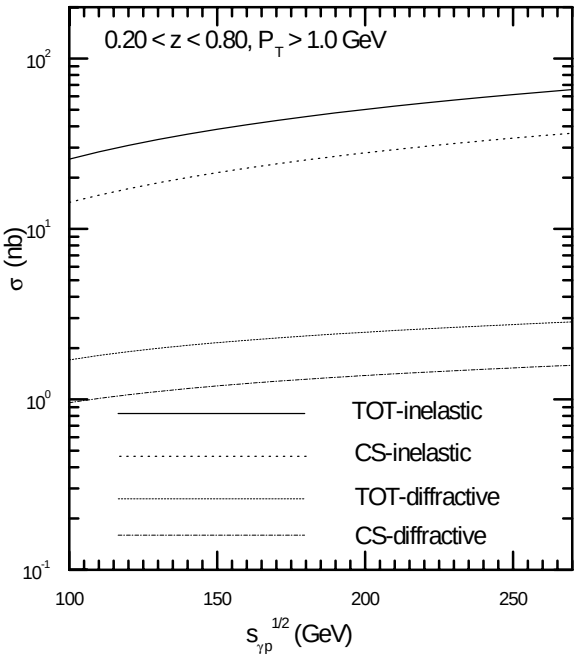

Fig. 5. Total J/ψ + jet photoproduction cross section for $P_{\rm T} \ge 1.0\,\mathrm{GeV}$, $0.2 \le z \le 0.8$, as a function of $s_{\gamma p}^{1/2}$. The thin dash-dotted and short dashed lines represent the color-singlet contribution and the sum of the color-singlet and color-octet contributions to J/ψ + jet diffractive photoproduction $\gamma + p \to J/\psi + \mathrm{jet} + p + X$, respectively. The thick solid and dotted lines curves are the sum of the color-singlet and color-octet contributions and the color-singlet contribution to inelastic J/ψ + jet photoproduction $\gamma + p \to J/\psi + \mathrm{jet} + X$, respectively

energy region considered the color-singlet contribution is about the order of 10^0 nb, so this process is measurable at DESY HERA.

Recently, it was pointed out that the cross section with an additional z cut, say, $z \le 0.9$, *cannot* be reliably predicted in NRQCD [37,47], because the NRQCD expansion is singular at $z = 1$. Only an average cross section over a sufficiently large region close to $z = 1$ can be predicted. To reliably predict the z distribution in the z region close to the boundary of phase space requires additional non-perturbative information in the form of so-called shape functions. These shape functions are also required to predict the $P_{\rm T}$ distributions with an additional upper z cut, say, $z \le 0.9$, but not if z is integrated up to its kinematic maximum. So in Fig. 6, we show the $P_{\rm T}$ distribution $\mathrm{d}\sigma/\mathrm{d}P_{\rm T}$ at HERA at $s_{\gamma p}^{1/2} = 100\,\mathrm{GeV}$ where z is integrated from its lower cut 0.2 to its kinematic maximum. The codes for the curves are the same as Fig. 4. We find that for the J/ψ+jet diffractive production in process (1), without the upper z cut, the color-octet contributions are dominant in the whole $P_{\rm T}$ region considered; they exceed the color-singlet contribution by almost an order of magnitude. In Fig. 7, the cross sections of the diffractive J/ψ+jet production in direct photon processes as a function of $s_{\gamma p}^{1/2}$ for $P_{\rm T} \ge 1.0$ GeV, $0.2 \le z \le z_{\max}$, are shown. We observe that in the energy region considered the color-singlet contribution is in the region $1.4\,\mathrm{nb} < \sigma^{\mathrm{diff.}}(\mathrm{singlet}) < 2.4\,\mathrm{nb}$, while including the color-octet contributions the cross section increased by about an order of magnitude. So, the experimental measurement of the $P_{\rm T}$ distribution and the total cross section with cuts $P_{\rm T} > 1.0\,\mathrm{GeV}$, $z \ge 0.2$, will give a stringent test of these statements based on the color-octet mechanism.

So far, we presented a study of the J/ψ diffractive production at large $P_{\rm T}$ in the direct photon processes at HERA based on the factorization theorem for lepton-induced hard diffractive scattering. However, there are so-called resolved photon processes which contribute to J/ψ diffractive production at large $P_{\rm T}$. The diffractive factorization breaks down for the resolved photon processes [11]. It may be difficult to tell in practice if there are some photon remnants present in an event, so the contributions from the direct and resolved processes might be difficult to separate in an experimental signal for J/ψ diffractive production at large $P_{\rm T}$. In this case, the resolved photon processes contributions must be subtracted from the experimental data to obtain the direct photon processes contributions which we studied in this paper. First, we use a z cut, $z \ge 0.2$, to reduce backgrounds from the resolved photon processes [35,37]. Second, the Tevatron data on the diffractive production of jets, weak bosons, and b-quarks

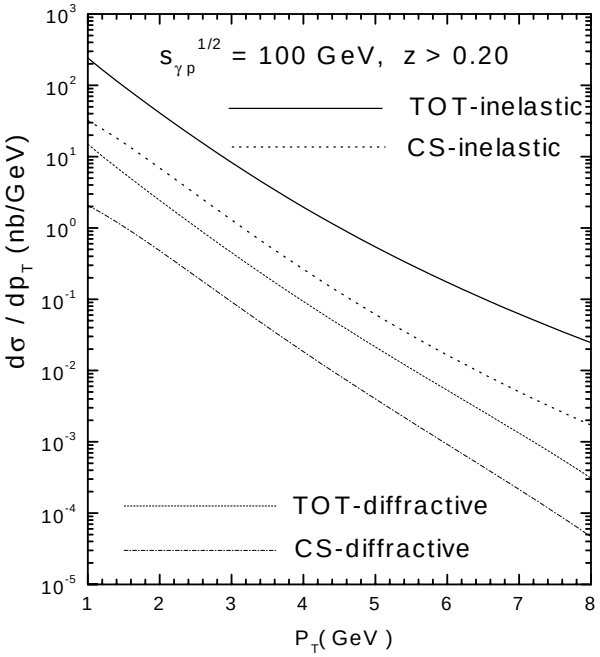

Fig. 6. Transverse momentum ($P_{\rm T}$) distribution $\mathrm{d}\sigma/\mathrm{d}P_{\rm T}$ for J/ψ + jet photoproduction at HERA at $s_{\gamma p}^{1/2} = 100\,\mathrm{GeV}$ with z integrated from its lower cut 0.2 to its kinematic maximum. The thin dash-dotted and short dashed lines represent the color-singlet contribution and the sum of the color-singlet and color-octet contributions to J/ψ + jet diffractive photoproduction $\gamma + p \to J/\psi + \mathrm{jet} + p + X$, respectively. The thick solid and dotted lines curves are the sum of the color-singlet and color-octet contributions and the color-singlet contribution to inelastic J/ψ + jet photoproduction $\gamma + p \to J/\psi + \mathrm{jet} + X$, respectively

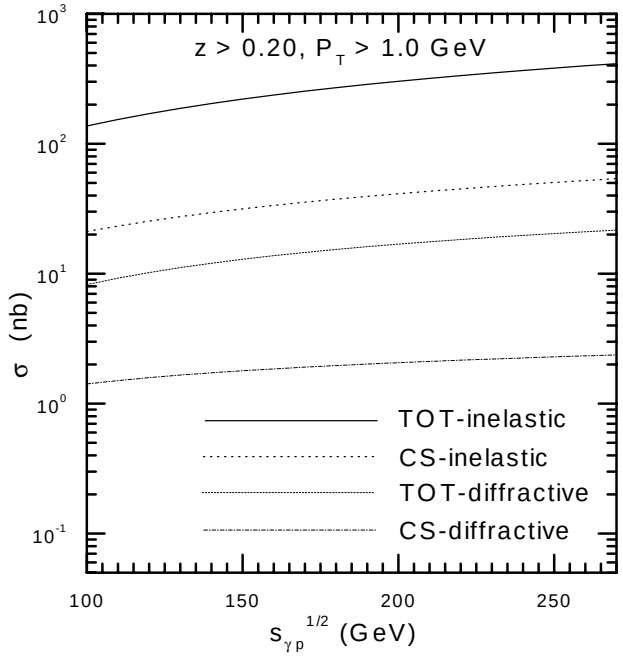

Fig. 7. Total J/ψ + jet photoproduction cross section for $P_{\rm T} \geq 1.0\,\mathrm{GeV}$, $z \geq 0.2$ as a function of $s_{\gamma p}^{1/2}$. The thin dash-dotted and short dashed lines represent the color-singlet contribution and the sum of the color-singlet and color-octet contributions to J/ψ + jet diffractive photoproduction $\gamma + p \to J/\psi + \mathrm{jet} + p + X$, respectively. The thick solid and dotted lines curves are the sum of the color-singlet and color-octet contributions and the color-singlet contribution to inelastic J/ψ+jet photoproduction $\gamma + p \to J/\psi + \mathrm{jet} + X$, respectively

[9] all indicate that the non-factorization effects can be taken into account by the so-called renormalization factor D (i.e. the rapidity gap survival probability) [48] which is dependent on the center of mass energy concerned. At the Tevatron energy ($s^{1/2} = 1.8\,\mathrm{TeV}$), the D factor is about 0.2. For diffractive dijet production at HERA, it is found that a rapidity gap survival probability of $0.4 \sim 0.6$ is needed to account for spectator interactions in resolved photon processes in order to obtain the best description of the combined DIS and photoprouction data [8]. Provided one takes into account non-factorization effects in this way, the remaining resolved photon processes contributions can be subtracted from the experimental data.

The non-diffractive background can be removed by performing the large rapidity gap analysis. The elastic (with or without proton dissociation) photoproduction of J/ψ falls exponentially with t ($\simeq P_{\rm T}$ in elastic photoproduction) and the produced J/ψ mainly has $P_{\rm T} < 1.0\,\mathrm{GeV}$ [23,24]. This background can be dropped out by imposing a large $P_{\rm T}$ cut. In this paper we use $P_{\rm T} \geq 1.0\,\mathrm{GeV}$, and $|t| \leq 1.0\,\mathrm{GeV}^2$. If statistics is not a limitation, it might be preferable to use a larger $P_{\rm T}$ cut. Alternatively this background can be dropped out by the emergence of a "jet" with opposite transverse momentum in the main detector. After these cuts, a potentially important background to the process we studied comes from a competing diffractive production mechanism provided one does not know experimentally whether the diffractive final state contains the "Pomeron remnant". This is diffractive J/ψ production at large $P_{\rm T}$ in the perturbative two-gluon exchange model. In the perturbative two-gluon exchange model, the diffractive final state is more exclusive, contains no "Pomeron remnant", and the two gluons in a net color-singlet with quantum numbers $P = 0$, $C = 0$, couple in all possible ways to the $|c\bar{c}g\rangle$ Fock state of the photon in the proton rest frame. Furthermore, in the perturbative two-gluon exchange model, at leading order, due to C-invariance, only color-octet $(c\bar{c})[^3P_J^{(8)}, J = 0,1,2]$ and $(c\bar{c})[^1S_0^{(8)}]$ intermediate states contribute to diffractive J/ψ production at large $P_{\rm T}$; hence the J/ψ produced through these color-octet intermediate states is expected to be always accompanied by light hadrons. The most distinctive feature of this model is that the amplitude is related to the so-called off-diagonal gluon distribution function [49], hence at HERA, the cross section is expected to rise with $s_{\gamma p}^{1/2}$ with a steep, scale dependent power, and the slope of the t distribution is expected to have no shrinkage. This diffractive production mechanism certainly deserves to be studied in detail, but is beyond the scope of this paper. Precise measurements of the energy dependence and the t slope of this process is needed in order to find out which mech-

anism gives a dominant contribution to J/ψ diffractive production at large $P_{\rm T}$.

In conclusion, in this paper we present a study of the J/ψ + jet diffractive production in the direct photon process at HERA based on the factorization theorem for lepton-induced hard diffractive scattering and the factorization formalism of the non-relativistic QCD (NRQCD) for quarkonia production. Using the diffractive gluon distribution function extracted from HERA data on diffractive deep inelastic scattering and diffractive dijet photon production, we demonstrate that this process is measurable at DESY HERA. The experimental study of this process can give valuable insights in the diffractive production mechanism and test the color-octet mechanism for heavy quarkonia production in a new environment.

Acknowledgements. This work is supported in part by the National Natural Science Foundation of China, Doctoral Program Foundation of Institution of Higher Education of China and Hebei Province Natural Science Foundation, China.

A The spin, color average-squared matrix elements

In this appendix, we give explicit expressions for the spin and color average-squared matrix elements of photon–gluon fusion subprocesses. The results are obtained using the symbolic manipulations with the aid of REDUCE package.

$$\overline{\Sigma}|M(\gamma+g\to(c\bar{c})[^3S_1^{(1)}]+g)|^2=\frac{64}{12}(ee_cg_s^2)^2m_\psi^2 \times\frac{\hat{s}^2(\hat{t}+\hat{u})^2+\hat{t}^2(\hat{s}+\hat{u})^2+\hat{u}^2(\hat{s}+\hat{t})^2}{(\hat{t}+\hat{u})^2(\hat{s}+\hat{u})^2(\hat{u}+\hat{t})^2} \tag{24}$$

$$\overline{\Sigma}|M(\gamma+g\to(c\bar{c})[^3S_1^{(8)}]+g)|^2=\frac{15}{6}\overline{\Sigma}|M(\gamma+g\to(c\bar{c})[^3S_1^{(1)}]+g)|^2 \tag{25}$$

$$\begin{aligned}&\overline{\Sigma}|M(\gamma+g\to(c\bar{c})[^1S_0^{(8)}]+g)|^2\\&=\frac{24\hat{s}\hat{u}(ee_cg_s^2)^2}{\hat{t}(\hat{s}+\hat{t})^2(\hat{s}+\hat{u})^2(\hat{t}+\hat{u})^2}\\&\times(\hat{s}^4+2\hat{s}^3\hat{t}+2\hat{s}^3\hat{u}+3\hat{s}^2\hat{t}^2+6\hat{s}^2\hat{t}\hat{u}+3\hat{s}^2\hat{u}^2+2\hat{s}\hat{t}^3\\&+6\hat{s}\hat{t}^2\hat{u}+6\hat{s}\hat{t}\hat{u}^2+2\hat{s}\hat{u}^3+\hat{t}^4+2\hat{t}^3\hat{u}+3\hat{t}^2\hat{u}^2\\&+2\hat{t}\hat{u}^3+\hat{u}^4)\\&=\frac{24\hat{s}\hat{u}(eecg_s^2)^2}{\hat{t}(\hat{s}+\hat{t})^2(\hat{s}+\hat{u})^2(\hat{t}+\hat{u})^2}\{[\hat{u}^2+(\hat{s}+\hat{u}+\hat{t})(\hat{s}+\hat{t})]^2\\&-2\hat{s}\hat{t}(\hat{s}+\hat{t})^2+\hat{s}^2\hat{t}^2\}\end{aligned} \tag{26}$$

$$\begin{aligned}&\sum_J\overline{\Sigma}|M(\gamma+g\to(c\bar{c})[^3P_J^{(8)}]+g)|^2\\&=\frac{96(ee_cg_s^2)^2}{\hat{t}m_\psi^2(\hat{s}+\hat{t})^3(\hat{s}+\hat{u})^3(\hat{t}+\hat{u})^3}\\&\times(7\hat{s}^7\hat{t}\hat{u}+7\hat{s}^7\hat{u}^2+25\hat{s}^6\hat{t}^2\hat{u}\\&+38\hat{s}^6\hat{t}\hat{u}^2+21\hat{s}^6\hat{u}^3+2\hat{s}^5\hat{t}^4\\&+47\hat{s}^5\hat{t}^3\hat{u}+88\hat{s}^5\hat{t}^2\hat{u}^2+78\hat{s}^5\hat{t}\hat{u}^3\\&+35\hat{s}^5\hat{u}^4+4\hat{s}^4\hat{t}^5+63\hat{s}^4\hat{t}^4\hat{u}+132\hat{s}^4\hat{t}^3\hat{u}^2+156\hat{s}^4\hat{t}^2\hat{u}^3\\&+98\hat{s}^4\hat{t}\hat{u}^4+35\hat{s}^4\hat{u}^5+2\hat{s}^3\hat{t}^6+47\hat{s}^3\hat{t}^5\hat{u}\\&+136\hat{s}^3\hat{t}^4\hat{u}^2+190\hat{s}^3\hat{t}^3\hat{u}^3+156\hat{s}^3\hat{t}^2\hat{u}^4+78\hat{s}^3\hat{t}\hat{u}^5\\&+21\hat{s}^3\hat{u}^6+13\hat{s}^2\hat{t}^6\hat{u}+70\hat{s}^2\hat{t}^5\hat{u}^2+136\hat{s}^2\hat{t}^4\hat{u}^3\\&+132\hat{s}^2\hat{t}^3\hat{u}^4+88\hat{s}^2\hat{t}^2\hat{u}^5+38\hat{s}^2\hat{t}\hat{u}^6+7\hat{s}^2\hat{u}^7\\&+13\hat{s}\hat{t}^6\hat{u}^2+47\hat{s}\hat{t}^5\hat{u}^3+63\hat{s}\hat{t}^4\hat{u}^4+47\hat{s}\hat{t}^3\hat{u}^5\\&+25\hat{s}\hat{t}^2\hat{u}^6+7\hat{s}\hat{t}\hat{u}^7+2\hat{t}^6\hat{u}^3+4\hat{t}^5\hat{u}^4+2\hat{t}^4\hat{u}^5)\end{aligned} \tag{27}$$

References

1. See, for instance, P.D.B. Collins, An introduction to Regge theory and high energy physics (Cambridge University Press, Cambridge 1977); A.B. Kaidalov, Phys. Rep. **50**, 157 (1979); K. Goulianos, Phys. Rep. **101**, 169 (1985)
2. F.E. Low, Phys. Rev. D **12**, 163 (1975); S. Nussinov, Phys. Rev. Lett. **34**, 1286 (1975); Phys. Rev. D **12**, 246 (1976)
3. G. Ingelman, P.E. Schlein, Phys. Lett. B **152**, 256 (1985)
4. UA8 Collaboration, A. Brandt et al., Phys. Lett. B **297**, 417 (1992); R. Bonino et al., ibid. **211**, 239 (1988)
5. ZEUS Collaboration, M. Derrick et al., Phys. Lett. B **315**, 481 (1993); **332**, 228 (1994); H1 Collaboration, T. Ahmed et al., Nucl. Phys. B **429**, 477 (1994)
6. ZEUS Collaboration, M. Derrick et al., Z. Phys. C **68**, 569 (1995); Phys. Lett. B **356**, 129 (1995); ZEUS Collaboration, J. Breitweg et al., Eur. Phys. J. **1**, 81 (1998); C **5**, 41 (1998); **6**, 43 (1999); ZEUS Collaboration, to appear in Proceedings of the International Europhysics Conference on High Energy Physics (Tampere, Finland, July 15–21, 1999, abstract 505)
7. H1 Collaboration, C. Adloff et al., Z. Phys. C **76**, 613 (1997); Phys. Lett. B **428**, 206 (1998); Eur. Phys. J. C **1**, 495 (1998); **5**, 439 (1998); H1 Collaboration, S. Aid et al., Z. Phys. C **70**, 609 (1996)
8. H1 Collaboration, C. Adloff et al., Eur. Phys. J. C **6**, 421 (1999)
9. CDF Collaboration, F. Abe et al., Phys. Rev. Lett. **78**, 2698 (1997); **79**, 2636 (1997); CDF Collaboration, T. Affolder et al., FERMILAB-PUB-99/229-E
10. For some recent reviews, see A. Goussiou et al., in Proceedings of the 6th International Workshop on Deep Inelastic Scattering and QCD (DIS98), Brussels, 1998, p. 287; H. Jung, DESY 98-130, 1998; H. Abramowicz, A. Caldwell, DESY 98-192, 1998; D.M. Jansen, M. Albrow, R. Brugnera, hep-ph/9905537; M. Diehl, hep-ph/9906518
11. J.C. Collins, Phys. Rev. D **57**, 3051 (1998)
12. Z. Kunszt, W.J. Stirling, in Proceedings of the International Workshop on Deep Inelastic Scattering and Related Phenomena (DIS 96), Rome, 1996, edited by G. D'Agostini, A. Nigro (World Scientific, Singapore 1997) p. 240; F. Hautmann, Z. Kunszt, D.E. Soper, Phys. Rev. Lett. **81**, 3333 (1998)
13. A. Berera, D.E. Soper, Phys. Rev. D **50**, 4328 (1994); **53**, 6162 (1996)
14. L. Alvero, J.C. Collins, J. Terron, J.J. Whitmore, Phys. Rev. D **59**, 074022 (1999)
15. A. Edin, G. Ingelman, J. Rathsman, Phys. Lett. B **366**, 371 (1996); G. Ingelman, DESY 99-009

16. N.N. Nikolaev, B.G. Zakharov, Z. Phys. C **53**, 331 (1992); M. Wüsthoff, Phys. Rev. D **56**, 4311 (1997); J. Bartels, M. Wüsthoff, J. Phys. G **22**, 929 (1996); S.J. Brodsky, P. Hoyer, L. Magnea, Phys. Rev. D **55**, 5585 (1997); A. Bialas, R. Peschanski, Phys. Lett. B **387**, 405 (1996); A. Bialas, R. Peschanski, C. Royon, Phys. Rev. D **57**, 6899 (1998)
17. J. Bartels, J. Ellis, H. Kowalski, M. Wüsthoff, Eur. Phys. J. C **7**, 443 (1999)
18. W. Buchmüller, M.F. McDermott, A. Hebecker, Nucl. Phys. B **487**, 283 (1997); ibid. 500, 621(E) (1997); W. Buchmüller, A. Hebecker, ibid. **476**, 203 (1996)
19. A. Hebecher, Nucl. Phys. B **505**, 349 (1997)
20. G.T. Bodwin, E. Braaten, G.P. Lepage, Phys. Rev. D **51**, 1125 (1995); ibid. 55, 5853(E) (1997)
21. W.E. Caswell, G.P. Lepage, Phys. Lett. B **167**, 437 (1986)
22. M.G. Ryskin, R.G. Roberts, A.D. Martin, E.M. Levin, Z. Phys. C **76**, 231 (1997); L. Frankfurt, W. Koepf, M. Strikman, Phys. Rev. D **57**, 512 (1997)
23. H1 Collaboration, S. Aid, et al., Nucl. Phys. B**472**, 3 (1996), C. Adloff, et al., Eur. Phys. J. C **10**, 373 (1999)
24. ZEUS Collaboration, J. Breitweg, et al., Z. Phys. C **75**, 215 (1997)
25. H. Jung, D. Krücker, C. Greub, D. Wyler, Z. Phys. C **60**, 721 (1993)
26. Chao-Hsi Chang, Nucl. Phys. B **172**, 425 (1980); E.L. Berger, D. Jones, Phys. Rev. D **23**, 1512 (1981); R. Baier, R. Rukel, Z. Phys. C **19**, 251 (1983)
27. For some recent reviews, see E. Braaten, S. Fleming, T.C. Yuan, Ann. Rev. Nucl. Part. Sci. **46**, 197 (1996); E. Braaten, hep-ph/9702225; hep-ph/9810390; M. Beneke, hep-ph/9703429; and references therein
28. CDF Collaboration, F. Abe et al., Phys. Rev. Lett. **79**, 572 (1997); ibid., **79**, 578 (1997)
29. E. Braaten, T.C. Yuan, Phys. Rev. Lett. **71**, 1673 (1993)
30. E. Braaten, M.A. Doncheski, S. Fleming, M. Mangano, Phys. Lett. B **333**, 548 (1994); M. Cacciari, M. Greco, Phys. Rev. Lett. **73**, 1586 (1994); D.P. Roy, K. Sridhar, Phys. Lett. B **339**, 141 (1994)
31. E. Braaten, S. Fleming, Phys. Rev. Lett. **74**, 3327 (1995)
32. P. Cho, A.K. Leibovich, Phys. Rev. D **53**, 6203 (1996); ibid. **53**, 150 (1996)
33. M. Beneke, M. Krämer, Phys. Rev. D 55, R5269 (1997)
34. G.P. Lepage, et al., Phys. Rev. D **46**, 4052 (1992)
35. P. Ko, Jungil Lee, H.S. Song, Phys. Rev. D **54**, 4312 (1996)
36. M. Cacciari, M. Krämer, Phys. Rev. Lett. **76**, 4128 (1996)
37. M. Beneke, M. Krämer, M. Vänttinen, Phys. Rev. D **57**, 4258 (1998)
38. S. Fleming, T. Mehen, Phys. Rev. D **57**, 1846 (1998)
39. ZEUS Collaboration, J. Breitweg, et al., Z. Phys. C **76**, 599 (1997)
40. B.A. Kniehl, G. Krämer, Eur. Phys. J. C **6**, 493 (1999); K. Sridhar, A.D. Martin, W.J. Stirling, Phys. Lett. B **438**, 211 (1998)
41. A. Edin, G. Ingelman, J. Rathsman, Phys. Rev. D **56**, 7317 (1997); J.F. Amundson, O.J.P. Eboli, E.M. Gregores, F. Halzen, Phys. Lett. B **390**, 323 (1997) and references therein; O.J.P. Eboli, E.M. Gregores, F. Halzen, hep-ph/9901387
42. See, for instance, R.D. Field, Applications of Perturbative QCD (Addison-Wesley Publishing Company, Inc. 1989); G. Sterman et al., Rev. Mod. Phys. **67**, 157 (1995)
43. W. Buchmüller, S. -H.H. Tye, Phys. Rev. D **24**, 132 (1981)
44. E.J. Eichten, C. Quigg, Phys. Rev. D **52**, 1726 (1995)
45. B. Cano-Coloma, M.A. Sanchis-Lozano, Nucl. Phys. B **508**, 753 (1997); M.A. Sanchis-Lozano, hep-ph/9907497
46. M. Glück, E. Reya, A. Vogt, Z. Phys. C **67**, 433 (1995)
47. M. Beneke, I.Z. Rothstein, M.B. Wise, Phys. Lett. B **408**, 373 (1997)
48. K. Goulianos, Phys. Lett. B **358**, 379 (1995); 363, 268(E) (1995); K. Goulianos, J. Montanha, Phys. Rev. D **59**, 114017 (1999)
49. X. Ji, Phys. Rev. Lett. **78**, 610 (1997); Phys. Rev. D **55**, 7114 (1997); J. Phys. G **24**, 1181 (1998); A.V. Radyushkin, Phys. Lett. B **380**, 417 (1996); ibid., **385**, 333 (1996)